

# Fast Method for Calculating Spatially Resolved Heterogeneous Electron-Transfer Kinetics and Its Application to Graphene with Defects

Sergey V. Pavlov, Vitaliy A. Kislenko, and Sergey A. Kislenko\*

Cite This: <https://dx.doi.org/10.1021/acs.jpcc.0c05376>

Read Online

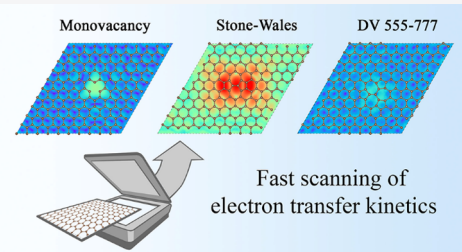
ACCESS |

Metrics &amp; More

Article Recommendations

Supporting Information

**ABSTRACT:** Establishing the relationship between the electrochemical activity of a surface and its chemical structure is extremely important for the development of new functional materials for electrochemical energy conversion systems. Here, we present a fast method, which combines a theoretical model and density functional theory calculations, for the prediction of nonadiabatic electron-transfer kinetics at nanoscale surfaces with spatial resolution. We propose two approaches for the calculation of electronic coupling, which characterizes the interaction strength between electronic states of a redox-active molecule and surface electronic states and depends on the position of the molecule above the surface. The first one is based on the linear approximation between the electronic coupling and overlap integral and takes into account the molecular wave function explicitly. The second one uses Tersoff–Hamann and Chen approximations that are based on the model assumption about the molecular orbital structure and allow ultrafast electron-transfer kinetic calculations only from the surface wave function. The proposed method was applied for the electron-transfer kinetic investigation of graphene with defects. We have shown that defects can act as electrocatalytic sites, selectively increasing the electron-transfer rate in a different range of standard redox potentials depending on the defect type.



## INTRODUCTION

Heterogeneous electron transfer (ET) at the electrode surface is an essential process in electrochemistry from both a fundamental and an application point of view. ET forms the basis of such important applications as fuel cells,<sup>1</sup> electrochemical conversion of CO<sub>2</sub>,<sup>2</sup> water splitting,<sup>3,4</sup> and rechargeable batteries.<sup>5,6</sup> High practical importance has stimulated ongoing experimental and theoretical studies of the kinetics of this process for developing new electrocatalysts.<sup>7</sup>

One of the critical parameters determining the electron-transfer rate is the degree of interaction of the reactant with the surface, which is characterized by the electronic coupling parameter  $H_{if}$ .<sup>8</sup> If the interaction is strong, the electron transfer occurs in the adiabatic regime, which is preferable for the reaction at metal surfaces. In the case of a weak interaction, a nonadiabatic regime of electron transfer occurs, the theory of which is successfully used for the description of electron-transfer kinetics at semiconductor surfaces.<sup>9,10</sup>

Recently, studies of nonmetallic electrocatalysts based on chemically modified graphenes, as a cheaper alternative to platinum catalysts, have become widespread.<sup>4,11–13</sup> For example, doping graphene with various heteroatoms (N, P, S) or functionalization with oxygen-containing groups leads to increased catalytic activity in the oxygen reduction reaction.<sup>14</sup> The regime of electron transfer at the surface of carbon materials is still a subject of controversy.<sup>15–18</sup> In favor of the nonadiabatic transfer at the graphene surface, some exper-

imental studies can be highlighted, showing the growth of the rate constant for such chemical modifications that lead to an increase in the density of electronic states at the Fermi level; for example, acceleration of the ET at the graphene surface with vacancies,<sup>19</sup> and at graphene edges,<sup>20</sup> with an increase in the number of graphene layers.<sup>21</sup> For the directed design of such materials, it is necessary to understand the relationships between structural modifications and the kinetics of electrochemical processes.

On the one hand, to solve this problem, experimental methods are being developed, such as scanning electrochemical microscopy,<sup>22–26</sup> which allows investigating the electrochemical activity of materials with spatial resolution. For instance, the increased activity of graphene edges using Ru(NH<sub>3</sub>)<sub>6</sub><sup>3+/2+</sup> as a redox probe was shown.<sup>20</sup> In ref 27, the authors managed to obtain electrochemical current maps of single-walled carbon nanotubes. They found that the activity is greatly enhanced at kinked sites and regions modified by oxidation.<sup>27</sup> However, the spatial resolution of such studies is on the order of 100 nm, which limits their effectiveness for the

Received: June 13, 2020

Revised: July 21, 2020

Published: July 26, 2020

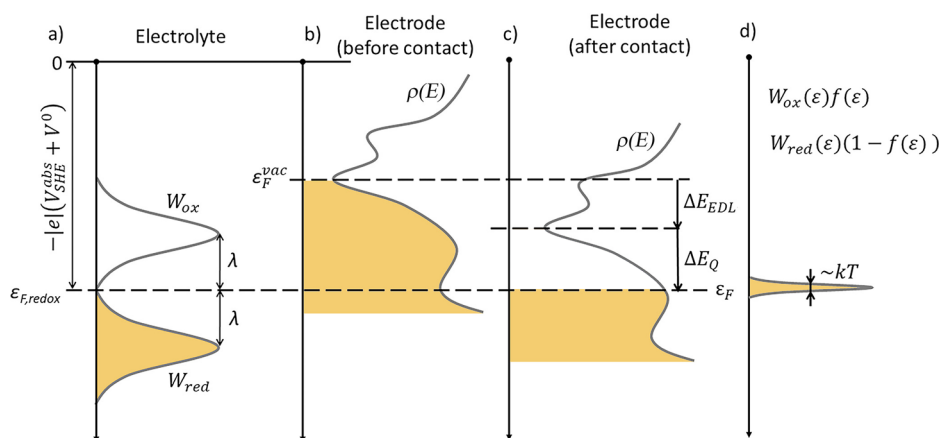


**Figure 1.** Energy diagram showing the alignment and occupation of electronic states in the electrode and electrolyte before and after equilibration. Occupied states are marked in yellow color.

study of point defects with a characteristic size of less than 1 nm.

In this regard, theoretical approaches for evaluating ET kinetics, using data from quantum chemical calculations as parameters, are of particular relevance. In our recent work, within the framework of the Gerischer theory, we examined the influence of the density of electronic states of graphene on electron transfer. We have shown the possibility of selective electrocatalysis of redox processes in a particular range of redox potentials depending on the type of defect.<sup>28</sup> However, this model did not take into account the effect of the electronic coupling matrix element  $H_{ij}$ , which depends on the position of the redox species above the surface and therefore is of great interest. The calculation of the electron transfer with a spatial resolution, taking into account electronic coupling, was performed by us earlier for the cluster density functional theory (DFT) simulations.<sup>29</sup> However, the use of this approach to study redox processes on point defects in real surfaces is limited because of edge effects.

The calculation of the electronic coupling is a fairly nontrivial problem. There are quite a few different approaches based both on wave function-based quantum chemical methods, such as generalized Mulliken–Hush (GMH) and fragment charge difference (FCD), and DFT-based approaches, such as frozen-density embedding (FDE) formalism, constrained DFT (CDFT), and fragment orbital DFT (FODFT).<sup>30,31</sup> Some of these approaches are implemented as standard methods in quantum chemical software packages.<sup>30</sup> Most of these methods have been successfully applied to the homogeneous charge transfer from a molecule to a molecule. There are also attempts to implement some approaches for periodic systems, where the quantum mechanical problem is solved in the plane-wave basis.<sup>32,33</sup> In the latter case, the calculation of the electronic coupling matrix element becomes quite computationally costly because of a large number of electronic states in plane-wave DFT. Also, noteworthy are works on heterogeneous electron transfer, which uses methods based on perturbation theory.<sup>34</sup> However, in this case, the calculation efficiency also does not allow obtaining the electron-transfer rate constant with a spatial resolution easily.

In this article, we propose two fast and flexible approaches for calculating the rate constant of the outer-sphere non-adiabatic electron transfer at nanoscale electrodes. The first one is more rigorous and based on the linear approximation,

according to which the electronic coupling is equal (up to a constant) to the overlap integral between donor and acceptor orbitals. In this case, the acceptor orbital of redox species explicitly takes into account for fast numerical overlap calculations on the grid. In the second approach, we propose to use analytical approximations that have been successfully approved for obtaining simulated scanning tunneling microscopy (STM) images from plane-wave DFT calculations. In this case, the electronic coupling can be assessed rapidly only from the surface wave function (using some assumptions about the wave function structure of redox-active species). As we focus on the nonadiabatic transfer regime at nanostructured semiconductor or semimetal electrodes with a low density of electronic states, our model takes into account the quantum capacitance of the surface for the correct prediction of the alignment and occupation of electronic states upon contact with an electrolyte.<sup>28,35</sup> To test the proposed approaches, we analyze the electron transfer on the surface of graphene containing various point defects. As a part of our work, a program code has been developed for calculating the electron-transfer rate constant based on the electronic properties of the surface obtained in Vienna Ab Initio Simulation Package (VASP).<sup>36,37</sup> The code is publicly available on GitHub.<sup>38</sup>

## THEORY

The rate constant of heterogeneous electron transfer at zero overpotential and under standard conditions (standard rate constant) from an electrode to a redox molecule placed at  $\vec{r}$  in solution in the nonadiabatic regime can be written as an integral over electron transitions from various levels  $\varepsilon$  in the electrode<sup>39,40</sup>

$$k(\vec{r}) = \int_{-\infty}^{\infty} \kappa(\varepsilon, \vec{r}) \frac{\omega}{2\pi} \exp\left(-\frac{(\varepsilon - \varepsilon_F - \lambda)^2}{4k_B T \lambda}\right) f(\varepsilon) \rho(\varepsilon) d\varepsilon \quad (1)$$

where  $f(\varepsilon)$  and  $\rho(\varepsilon)$  are the Fermi distribution function and density of electronic states (DOS) in the electrode, respectively;  $\omega$  is the effective frequency of fluctuations of the solvent polarization;  $\kappa(\varepsilon, \vec{r})$  is the electronic transmission coefficient, which characterizes the transition probability in the activated state from level  $\varepsilon$  to the acceptor state of the oxidized species in the solution;  $\lambda$  is the solvent reorganization energy; and  $\varepsilon_F$  is the Fermi energy of the electrode, which is equal to

the electrochemical potential of electrons in solution  $\varepsilon_{F,\text{redox}}$  at equilibrium.

According to the Landau–Zener theory,<sup>41,42</sup> the electronic transmission coefficient for the nonadiabatic reaction can be expressed as<sup>40</sup>

$$\kappa(\varepsilon, \vec{r}) = \frac{2\pi^{3/2} |H_{if}(\varepsilon, \vec{r})|^2}{\hbar\omega\sqrt{\lambda kT}} \quad (2)$$

Equations 1 and 2 can be rewritten in the form of Gerischer integral,<sup>43</sup> which allows a simple graphical interpretation

$$k(\vec{r}) = \frac{2\pi}{\hbar} \int_{-\infty}^{\infty} |H_{if}(\varepsilon, \vec{r})|^2 W_{\text{ox}}(\varepsilon) f(\varepsilon) \rho(\varepsilon) d\varepsilon \quad (3)$$

where  $W_{\text{ox}}(\varepsilon)$  is the energy distribution of oxidized states of a redox couple in solution, shown in Figure 1a

$$W_{\text{ox}}(\varepsilon) = \frac{1}{\sqrt{4\pi k_B T \lambda}} \exp\left\{-\frac{(\varepsilon - \varepsilon_{F,\text{redox}} - \lambda)^2}{4k_B T \lambda}\right\}$$

Thus, in the Gerischer model, the electron transfer can be treated as a process occurring between isoenergetic levels in contact phases. Reduction occurs from occupied states in the electrode to empty states in the redox system. The reverse process occurs from occupied states in the redox system ( $W_{\text{red}}$  in Figure 1a) to empty states of the solid.

To define the position of the energy level  $\varepsilon_{F,\text{redox}}$  we use the concept of the absolute electrode potential, according to which a point in vacuum close to the surface of the solution is taken as the reference (zero) level.<sup>44</sup> Then,  $\varepsilon_{F,\text{redox}}$  can be calculated from the absolute potential of the standard hydrogen electrode  $V_{\text{SHE}}^{\text{abs}}$  and the standard redox potential of a couple  $V^0$  vs standard hydrogen electrode (SHE)

$$\varepsilon_{F,\text{redox}} = -|e|(V_{\text{SHE}}^{\text{abs}} + V^0)$$

The value of  $-|e|V_{\text{SHE}}^{\text{abs}}$  was taken equal to  $-4.5$  eV.<sup>45</sup>

The position of an electrode band structure before contact with an electrolyte (Figure 1b) is defined by the Fermi energy level  $\varepsilon_{\text{F}}^{\text{vac}}$  of the uncharged surface relative to the point in a vacuum just outside the surface, which can be routinely estimated from DFT calculations.<sup>46</sup> Upon contact with the electrolyte, alignment of the Fermi level occurs due to charge exchange at the electrode/electrolyte interface. For the correct prediction of the level's shift and occupation in a nanostructured electrode with a low density of states, such as graphene, nanotubes, and semiconductor nanocrystals, the quantum capacitance must be taken into account.<sup>35</sup> A detailed description of the procedure has been given in our previous work.<sup>28</sup> Here, we briefly note that the quantum capacitance determines the Fermi level shift in the electrode relative to its band structure  $\Delta E_{\text{Q}}$ , while the double-layer capacitance  $C_{\text{EDL}}$  determines the band structure shift  $\Delta E_{\text{EDL}}$  as a whole ( $\Delta E_{\text{EDL}} = -|e|\sigma/C_{\text{EDL}}$ , where  $\sigma$  is the surface charge density obtained during an equilibration process). It can be seen from Figure 1c that

$$\varepsilon_{F,\text{redox}} - \varepsilon_{\text{F}}^{\text{vac}} = \Delta E_{\text{EDL}} - \Delta E_{\text{Q}} \quad (4)$$

Since the product  $W_{\text{ox}}(\varepsilon)f(\varepsilon)$  (or  $W_{\text{red}}(\varepsilon)(1-f(\varepsilon))$  for the reverse process) is nonzero in a very narrow energy range of  $\sim kT$  near  $\varepsilon_{\text{F}}$  (Figure 1d), only the levels near the Fermi energy contribute the most to the ET under zero overpotential.

In the current work, to obtain the spatially resolved electron-transfer rate constant, we focus on the calculation of the

electronic coupling matrix element  $H_{if}$ , which is a significant factor because it exponentially depends on the distance to the surface.<sup>29,34,47</sup> To calculate the matrix element, we use the linear approximation based on the Hückel theory,<sup>48</sup> according to which the matrix element is proportional to the overlap integral between the initial state  $\psi_i$  and the final state  $\psi_f$  of the transferred electron

$$H_{if}(\varepsilon, \vec{r}) = \langle \psi_i(\varepsilon) | \hat{H} | \psi_f(\vec{r}) \rangle \propto \langle \psi_i(\varepsilon) | \psi_f(\vec{r}) \rangle \quad (5)$$

This approach was approved in a number of works,<sup>49</sup> including ours, where the electron-transfer rate constant has been estimated from cluster DFT calculations with Gaussian-type orbitals (GTO).<sup>29,47</sup> Unlike ref 49, in which the authors calculate integrals of partially occupied molecular orbitals (POMOs) analytically, we used a numerical calculation of the overlap integral on a grid. In our case, we obtained wave functions of electrons in the electrode  $\psi_i(\varepsilon)$  from plane-wave DFT calculations for each energy  $\varepsilon$  and wave functions of the states in the redox-active molecule  $\psi_f$  from the Gaussian-type orbital DFT. We used a similar procedure in our recent work,<sup>29</sup> where the spatially resolved electron-transfer rate constant was calculated based on the results of DFT calculations in the GTO basis set, for both the electrode surface and redox species.

Besides this, in the current work, we propose to apply the simplified approach that is widely used for calculating scanning tunneling microscopy (STM) images from DFT calculations.<sup>50</sup> It is based on the use of the analytical approximation of the acceptor wave function  $\psi_f$ . Such an approximation was originally proposed by Tersoff and Hamann.<sup>51</sup> The idea is that  $\psi_f$  appears to be a spherical potential well (s-orbital). In such an approximation, it is shown that the energy-dependent electronic coupling matrix element is proportional to the surface wave function  $\psi_i$  of an electron with the corresponding energy  $\varepsilon$ , as shown in eq 6a

$$s: H_{if}(\varepsilon, \vec{r}) \propto \psi_i(\varepsilon, \vec{r}) \quad (6a)$$

$$p_z: H_{if}(\varepsilon, \vec{r}) \propto \frac{\partial}{\partial z} \psi_i(\varepsilon, \vec{r}) \quad (6b)$$

Then, this approach has been expanded to other types of orbitals (p,d) by Chen;<sup>52</sup> Equation 6b illustrates Chen's approximation for the  $p_z$  orbital. Expressions for other types of approximations can be found in ref 50. Computationally, such approximations allowed us not to calculate the overlap integral as in eq 5 for each position of the redox species above the surface, which is computationally quite costly, but immediately get the value of the electronic coupling (up to a constant), only from the value of the wave function or its derivative at the point  $\vec{r}$ .

Thus, our model contains the following variable parameters: the solvent reorganization energy  $\lambda$ , the standard redox potential  $V^0$ , the double-layer capacitance  $C_{\text{EDL}}$ , and a temperature  $T$ . The density of states  $\rho(\varepsilon)$ , the Fermi level  $\varepsilon_{\text{F}}^{\text{vac}}$ , and the surface wave functions  $\psi_i(\varepsilon)$  are taken from plane-wave DFT calculations.

The rate constant in eq 3 can be used for an exchange current density estimation across the whole interface

$$j_0 = \frac{e}{S} \int C(\vec{r}) k(\vec{r}) dV$$

where  $e$  is the charge of an electron,  $S$  is the surface area, and  $C(\vec{r})$  is the concentration distribution of the reactant at the

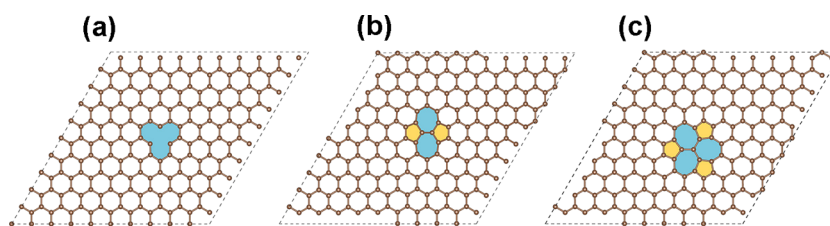


**Figure 2.** Model systems: (a) monovacancy, (b) Stone–Wales defect, and (c) double vacancy 555–777.

interface, which can be obtained from MD simulations, as in our previous works.<sup>53–55</sup>

## COMPUTATIONAL DETAILS

Plane-wave DFT calculations with periodic boundary conditions were performed using VASP.<sup>36,37</sup> The projector-augmented wave (PAW) method was used,<sup>56</sup> with the Perdew–Burke–Ernzerhof (PBE) exchange–correlation functional and the plane-wave cutoff energy was 500 eV. The van der Waals correction was not used. For ionic relaxation, we used a  $5 \times 5 \times 1$   $\Gamma$ -centered Monkhorst–Pack  $k$ -mesh. For calculating the electronic structure for further analysis, a  $k$ -mesh of  $33 \times 33 \times 1$  was used.

We considered three model systems, consisting of ca.  $2.5 \times 2.5$  nm<sup>2</sup> single-layer graphene and containing different point defects: single vacancy, Stone–Wales defect, and double vacancy 555–777 (Figure 2).

See technical details of data postprocessing in Section S2 of the Supporting Information. The procedure was implemented using Python 3 and is publicly available on GitHub.<sup>38</sup>

## RESULTS AND DISCUSSION

**Effect of the Acceptor Orbital Description.** In this section, we compare the results of the rate constant calculations from the two proposed approaches that differ in the acceptor orbital description for the electronic coupling estimation. We briefly recall that the first approach (more robust and time-consuming) explicitly takes into account the acceptor orbital structure obtained from a separate DFT simulation of an acceptor molecule. The second one uses Tersoff–Hamann and Chen approximations that are based on the model assumption about the acceptor orbital structure and allows fast ET kinetic calculation only from the surface wave function.

We examined the ET rate constant from the graphene surface with a single vacancy to the oxidized form of the following redox couples:  $\text{O}_2/\text{O}_2^-$ ,  $\text{Ru}(\text{NH}_3)_6^{3+/2+}$ , and  $\text{IrCl}_6^{2-/3-}$ . These couples were chosen due to their very different properties, such as the standard redox potentials (Table 1) and structures of the highest occupied molecular orbitals of the corresponding molecules in the reduced form calculated via DFT with the GTO basis set (Figures S1–S3). Technical details of these calculations are provided in Section S1 of the

Supporting Information. The following parameters were used:  $T = 300$  K and the double-layer capacitance was equal to the characteristic value  $20 \mu\text{F}/\text{cm}^2$ .<sup>57</sup> The calculations were done for the acetonitrile solvent, in which the oxygen reduction is a one-electron outer-sphere process.<sup>58,59</sup> The standard redox potentials and reorganization energies in acetonitrile are shown in Table 1.

Constant-height images of the electron-transfer rate constant (when the oxidized form of a couple is scanned over the surface at a constant distance to the surface) are shown in Figure 3. The distances were chosen to ensure the non-adiabatic regime of the electron transfer. In the case of  $s$  and  $p_z$  approximations of the acceptor orbitals, the distance between the surface and the scanning plane was  $4.5 \text{ \AA}$ . For the correct comparison between analytical approximations of orbitals and the real ones, the distances between the graphene plane and centers of molecules were chosen as follows:  $5 \text{ \AA}$  for  $\text{O}_2$  and  $6.9 \text{ \AA}$  for both  $\text{IrCl}_6$  and  $\text{Ru}(\text{NH}_3)_6$ . These distances provide the location of the area of maximum overlap—which corresponds to the region closest to the graphene surface atoms—of about  $4.5 \text{ \AA}$ .

As can be seen from Figure 3, the use of real acceptor orbitals makes the images more blurry due to the characteristic size of the corresponding orbitals. Asymmetry may also occur (as in the case of  $\text{Ru}(\text{NH}_3)_6^{3+/2+}$ ) associated with the specific orientation and structure of the acceptor molecule. However, the main characteristic features of the images obtained by the two approaches are preserved: (1) the characteristic size of the region with an increased electron-transfer constant; (2) the relative activity of the defect and the nearby surface. Besides this, the results for  $s$  and  $p_z$  approximations are approximately the same, which are consistent with STM results for these two approximations.<sup>50</sup>

From the obtained results, it can be concluded that the Tersoff–Hamann or Chen analytical approximation can be used for the express surface analysis to identify electrocatalytic sites and their relative activities, especially if the real acceptor orbital is close to one of the analytical ones. The use of the analytical approximation speeds up the rate constant calculations by 2–3 orders of magnitude (see Figure S6) since there is no need to consider the overlap integrals (eq S1) and the results are obtained only from the local value of the surface wave function or its derivatives. However, to obtain more accurate results, it is preferable to use direct numerical overlapping of donor and acceptor wave functions in the electrode and electrolyte, respectively.

**Spatially Resolved ET Kinetics at the Graphene Surface: Effect of Defects and Standard Redox Potentials.** This section is devoted to the study of the electron-transfer kinetics with a spatial resolution at the graphene surface with the following point defects: monovacancy, Stone–Wales defect, and double vacancy 555–777. In our recent work,<sup>28</sup> neglecting electronic coupling, we have

**Table 1.** Standard Redox Potentials  $V^0$  and Reorganization Energies  $\lambda$  in Acetonitrile for the Corresponding Redox Couples

redox couple	$V^0$ , V vs SHE	$\lambda$ , eV
$\text{O}_2/\text{O}_2^-$	$-0.6$ <sup>60</sup>	$1.7$ <sup>61</sup>
$\text{Ru}(\text{NH}_3)_6^{3+/2+}$	$0.1$ <sup>62</sup>	$0.8$ <sup>63</sup>
$\text{IrCl}_6^{2-/3-}$	$0.87$ <sup>62</sup>	$1.2$ <sup>64</sup>

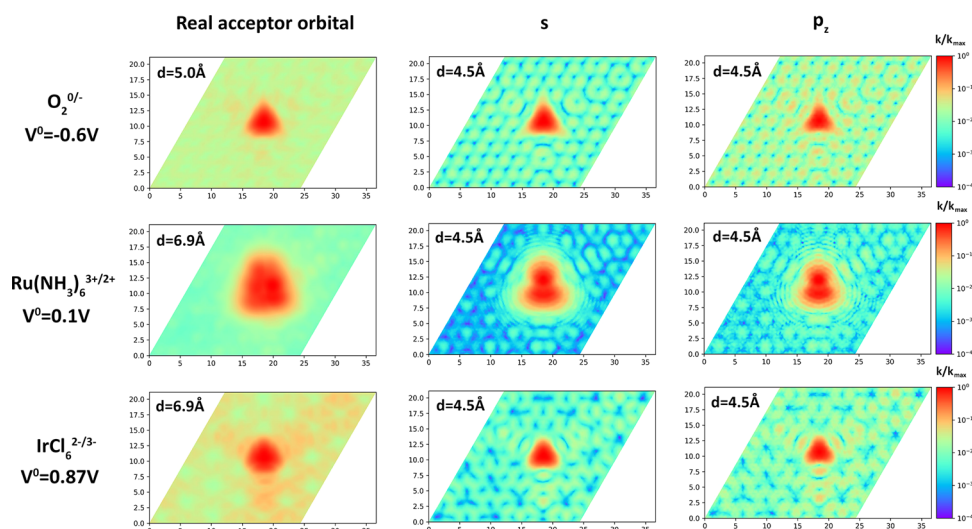


**Figure 3.** Constant-height images of the electron-transfer rate constant (in arbitrary units) at the graphene surface with vacancy defects for the corresponding redox couples depending on the level of description of the acceptor orbital.

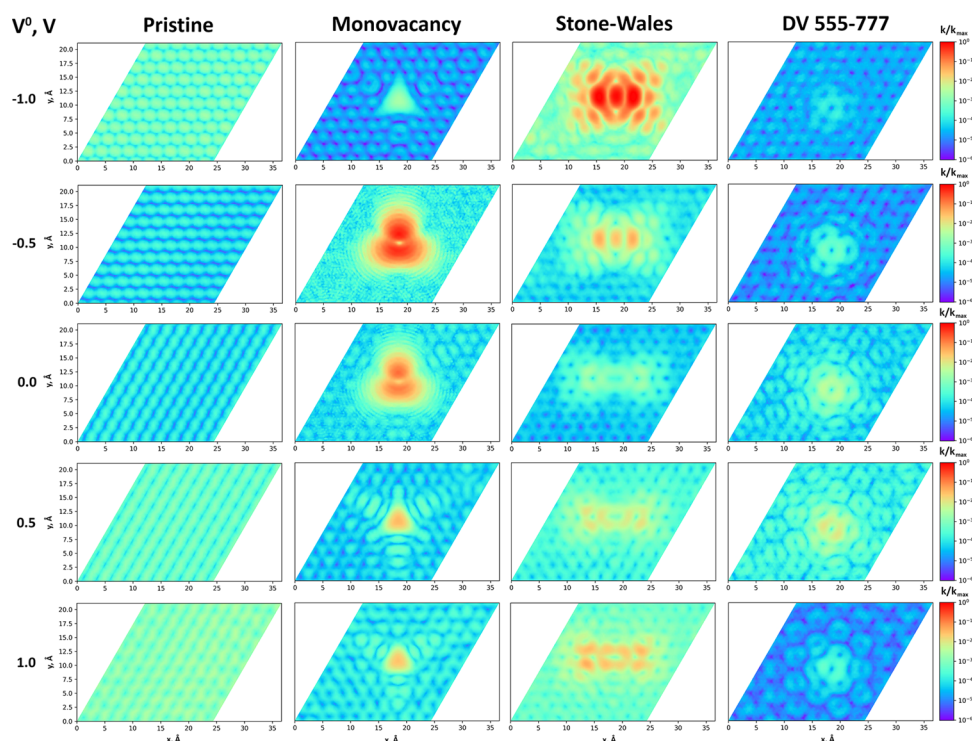


**Figure 4.** Constant-height images of the electron-transfer rate constant for different defects (columns) and standard redox potentials (rows).

shown semiquantitatively that different defects in graphene could increase the ET rate constant in different ranges of redox potentials, which opens the possibility for selective catalysis of electrochemical reactions. However, the question about spatially resolved reactivity of graphene with defects remained open, which we address in this section.

Here, we used the Tersoff–Hamann approximation (*s*-orbital). Constant-height images of the electron-transfer rate constant for different defects and standard redox potentials are shown in Figure 4. Scanning height is 4.5 Å. Since the Stone–Wales defect has a sine-wave-like shape, which is consistent with previous observations,<sup>65,66</sup> the results were averaged on both sides of the sheet.

It can be seen that pristine graphene has nearly uniform reactivity with slight corrugation reflecting the atomic structure. The surface-averaged rate constant largely depends on the redox potential. It can be explained by the Fermi level shift relative to the graphene band structure during equilibration with an electrolyte due to low quantum capacitance. As a result, under large redox potentials vs SHE, such as  $-1$  and  $+1$  V, the density of states  $\rho(\epsilon)$  at the Fermi level is increased (Figure 5a) and, as follows from eq 3, the rate constant is also increased. Redox-dependent electrochemistry of graphene has been previously observed experimentally.<sup>20</sup>

Defects lead to nonuniform electrochemical activity and act as catalytic sites (Figure 4). The local rate constant above defects can be 3 orders of magnitude larger than that above the

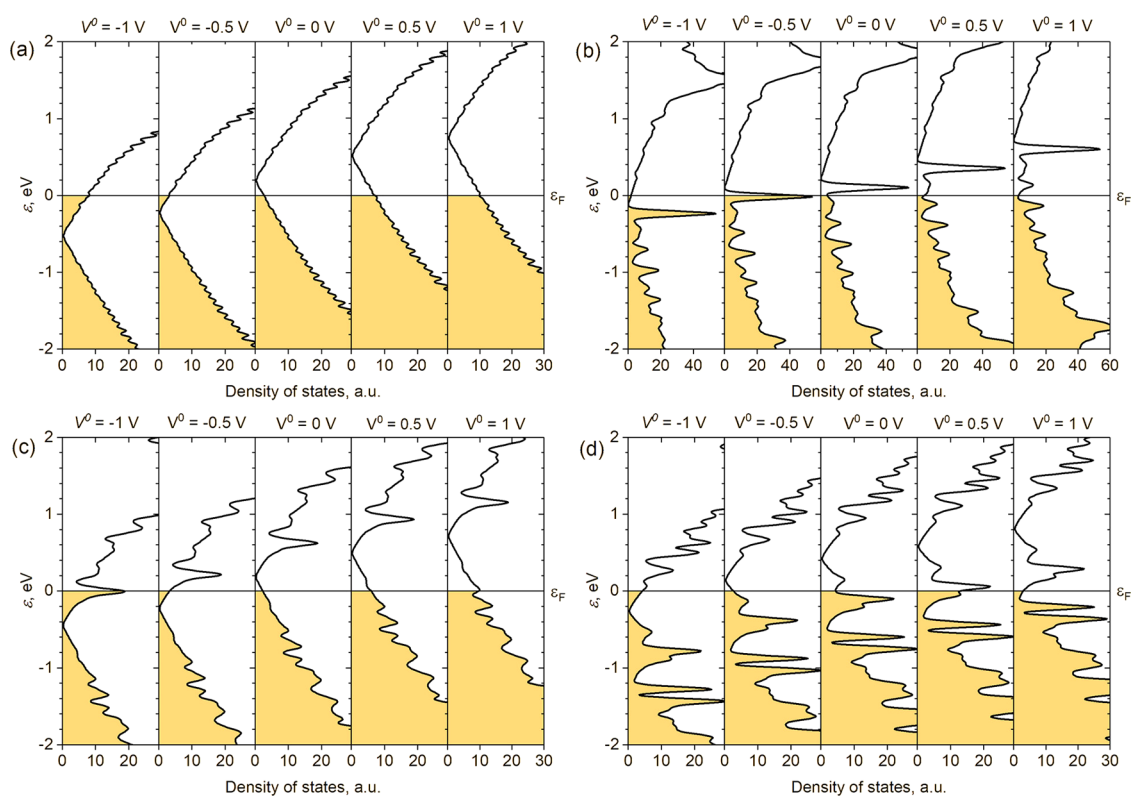


**Figure 5.** Energy diagram showing occupied electronic states of pristine graphene (a), graphene with vacancy (b), Stone–Wales defect (c), and double vacancy 555–777 (d).

nearby graphene surface, as in the vacancy case at  $V^0 = -0.5$  V. Similar to pristine graphene, the ET kinetics depends on the standard potential. However, the largest surface-averaged rate constant is observed at different  $V^0$  for different defects. Single vacancies accelerate the ET most strongly at  $V^0 = -0.5$  V, the Stone–Wales defects at  $V^0 = -1$  V, and double vacancies at  $V^0 = +0.5$  V. This selective effect is qualitatively explained by the fact that exactly at these potentials the density of states peaks, induced by defects, match the Fermi level after equilibration (Figure 5b–d). The nonuniform surface activity arises because the midgap states induced by defects are localized. Formation of localized states at vacancies and zigzag edges of graphene has been confirmed experimentally.<sup>67–69</sup> The shape and area of the increased ET rate vary depending on both the defect type and  $V^0$  and reflect the localized state structure near the Fermi level. For example, for monovacancy at the standard redox potential  $V^0 = +0.5$  V, the shape of a three-pointed star with sufficiently long rays is observed; meanwhile, at  $V^0 = -0.5$  V, this structure is not observed, and the area of the increased rate constant is localized almost inside the circle. The Stone–Wales defect shows the most delocalized states. The characteristic size of the area of the increased rate constant is more than 1 nm.

## CONCLUSIONS

In this article, we propose a fast method for assessing the electrocatalytic activity of surfaces based on plane-wave DFT calculations. The model takes into account the standard potential of a redox couple, the solvent reorganization energy, and the double-layer capacitance as variable parameters. The quantum capacitance of a nanosurface, which is determined by the density of states, is also considered for the correct

prediction of the alignment and occupation of electronic states upon contact with an electrolyte. We have proposed two approaches for the electronic coupling calculations. The first one is based on linear approximation, according to which the electronic coupling is proportional to the overlap integral between donor and acceptor orbitals. The second one utilizes Tersoff–Hamann and Chen approximations that are based on model assumptions about the acceptor orbital structure and allows ultrafast ET kinetic calculations only from the surface wave function. Constant-height images of the rate constant obtained by these approaches are similar. The main characteristic features of the images, such as the size of catalytic sites and their relative activity, are preserved. Our model has been applied for the ET kinetic investigation of graphene with defects (single vacancy, double vacancy, Stone–Wales defect). We have shown nonuniform electrochemical activity of graphene induced by the defects. The ET rate is increased above the defects. Different defects show the largest catalytic effect for different redox couples, what may be useful for applications in selective electrocatalysis and electrochemical sensors. The proposed method could also be applied to the electrode design for electrochemical energy conversion systems.

Finally, the limitations of the above approach are worth discussing. In the above formulated form, the model implies nonadiabaticity, i.e., weak overlapping of the wave functions between which electron transfer occurs. In principle, it is possible to expand this approach to the adiabatic regime of ET using the non-linearized version of eq 2 (see the Supporting Information for details) or even lowering of the activation energy could be taken into account, using, for example, the Newns–Anderson model.<sup>61,70</sup> However, it requires calibration

of the proportionality constant between the matrix element and the overlap integral (see eq 5), as, for instance, we did in our work<sup>29</sup> using the GMH method.

## ■ ASSOCIATED CONTENT

### SI Supporting Information

The Supporting Information is available free of charge at <https://pubs.acs.org/doi/10.1021/acs.jpcc.0c05376>.

Acceptor orbitals of redox species; technical details; computational efficiency; and non-linearized form of electronic transmission coefficient (PDF)

## ■ AUTHOR INFORMATION

### Corresponding Author

Sergey A. Kislenco – Joint Institute for High Temperatures, Moscow 125412, Russian Federation; [orcid.org/0000-0003-3579-5221](https://orcid.org/0000-0003-3579-5221); Email: [kislenco@ihed.ras.ru](mailto:kislenco@ihed.ras.ru)

### Authors

Sergey V. Pavlov – Joint Institute for High Temperatures, Moscow 125412, Russian Federation; Skolkovo Institute of Science and Technology, Moscow 143026, Russian Federation; [orcid.org/0000-0002-4221-9348](https://orcid.org/0000-0002-4221-9348)

Vitaliy A. Kislenco – Joint Institute for High Temperatures, Moscow 125412, Russian Federation

Complete contact information is available at: <https://pubs.acs.org/10.1021/acs.jpcc.0c05376>

### Notes

The authors declare no competing financial interest.

## ■ ACKNOWLEDGMENTS

The work was supported by a grant (No. 18-03-00773) from the Russian Foundation for Basic Research. The authors acknowledge the use of Zhores<sup>71</sup> for obtaining the results presented in this paper. The research was carried out using supercomputers at Joint Supercomputer Center of the Russian Academy of Sciences (JSCC RAS) and the equipment of the shared research facilities of HPC computing resources at Lomonosov Moscow State University.

## ■ REFERENCES

- (1) Liu, J.; Choi, H. J.; Meng, L. Y. A Review of Approaches for the Design of High-Performance Metal/Graphene Electrocatalysts for Fuel Cell Applications. *J. Ind. Eng. Chem.* **2018**, *64*, 1–15.
- (2) Jhong, H.-R. “Molly”; Ma, S.; Kenis, P. J. A. Electrochemical Conversion of CO<sub>2</sub> to Useful Chemicals: Current Status, Remaining Challenges, and Future Opportunities. *Curr. Opin. Chem. Eng.* **2013**, *2*, 191–199.
- (3) Joy, J.; Mathew, J.; George, S. C. Nanomaterials for Photoelectrochemical Water Splitting – Review. *Int. J. Hydrogen Energy* **2018**, *43*, 4804–4817.
- (4) Li, J.; Zhao, Z.; Ma, Y.; Qu, Y. Graphene and Their Hybrid Electrocatalysts for Water Splitting. *ChemCatChem* **2017**, *9*, 1554–1568.
- (5) Feng, N.; He, P.; Zhou, H. Critical Challenges in Rechargeable Aprotic Li-O<sub>2</sub> Batteries. *Adv. Energy Mater.* **2016**, *6*, 1502303–1502326.
- (6) Guo, X.; Sun, B.; Su, D.; Liu, X.; Liu, H.; Wang, Y.; Wang, G. Recent Developments of Aprotic Lithium-Oxygen Batteries: Functional Materials Determine the Electrochemical Performance. *Sci. Bull.* **2017**, *62*, 442–452.

- (7) Jiao, Y.; Zheng, Y.; Jaroniec, M.; Qiao, S. Z. Design of Electrocatalysts for Oxygen- and Hydrogen-Involving Energy Conversion Reactions. *Chem. Soc. Rev.* **2015**, *44*, 2060–2086.
- (8) Santos, E.; Nazmutdinov, R.; Schmickler, W. Electron Transfer at Different Electrode Materials: Metals, Semiconductors, and Graphene. *Curr. Opin. Electrochem.* **2020**, *19*, 106–112.
- (9) Memming, R. *Semiconductor Electrochemistry*; Wiley-VCH Verlag GmbH & Co. KGaA: Weinheim, Germany, 2015.
- (10) Kislenco, S.; Juarez, F.; Dominguez-Flores, F.; Schmickler, W.; Nazmutdinov, R. Tuning the Rate of an Outer-Sphere Electron Transfer by Changing the Electronic Structure of Carbon Nanotubes. *J. Electroanal. Chem.* **2019**, *847*, No. 113186.
- (11) Liu, X.; Dai, L. Carbon-Based Metal-Free Catalysts. *Nat. Rev. Mater.* **2016**, *1*, No. 16064.
- (12) Zhao, Q.; Mao, Q.; Zhou, Y.; Wei, J.; Liu, X.; Yang, J.; Luo, L.; Zhang, J.; Chen, H.; Chen, H.; Tang, L. Metal-Free Carbon Materials-Catalyzed Sulfate Radical-Based Advanced Oxidation Processes: A Review on Heterogeneous Catalysts and Applications. *Chemosphere* **2017**, *189*, 224–238.
- (13) Yan, Y.; Xia, B. Y.; Zhao, B.; Wang, X. A Review on Noble-Metal-Free Bifunctional Heterogeneous Catalysts for Overall Electrochemical Water Splitting. *J. Mater. Chem. A* **2016**, *4*, 17587–17603.
- (14) Hu, C.; Dai, L. Carbon-Based Metal-Free Catalysts for Electrocatalysis beyond the ORR. *Angew. Chem., Int. Ed.* **2016**, *55*, 11736–11758.
- (15) Nissim, R.; Batchelor-McAuley, C.; Henstridge, M. C.; Compton, R. G. Electrode Kinetics at Carbon Electrodes and the Density of Electronic States. *Chem. Commun.* **2012**, *48*, 3294–3296.
- (16) Luque, N. B.; Schmickler, W. Are the Reactions of Quinones on Graphite Adiabatic? *Electrochim. Acta* **2013**, *88*, 892–894.
- (17) Batchelor-McAuley, C.; Laborda, E.; Henstridge, M. C.; Nissim, R.; Compton, R. G. Reply to Comments Contained in “Are the Reactions of Quinones on Graphite Adiabatic?”, By N.B. Luque, W. Schmickler [Electrochim. Acta Xx (2012) Yyy]. *Electrochim. Acta* **2013**, *88*, 895–898.
- (18) Nazmutdinov, R. R.; Bronshtein, M. D.; Santos, E. Electron Transfer across the Graphene Electrode/Solution Interface: Interplay between Different Kinetic Regimes. *J. Phys. Chem. C* **2019**, *123*, 12346–12354.
- (19) Zhong, J.-H.; Zhang, J.; Jin, X.; Liu, J.-Y.; Li, Q.; Li, M.-H.; Cai, W.; Wu, D.-Y.; Zhan, D.; Ren, B. Quantitative Correlation between Defect Density and Heterogeneous Electron Transfer Rate of Single Layer Graphene. *J. Am. Chem. Soc.* **2014**, *136*, 16609–16617.
- (20) Güell, A. G.; Cuharuc, A. S.; Kim, Y. R.; Zhang, G.; Tan, S. Y.; Ebejer, N.; Unwin, P. R. Redox-Dependent Spatially Resolved Electrochemistry at Graphene and Graphite Step Edges. *ACS Nano* **2015**, *9*, 3558–3571.
- (21) Güell, A. G.; Ebejer, N.; Snowden, M. E.; Macpherson, J. V.; Unwin, P. R. Structural Correlations in Heterogeneous Electron Transfer at Monolayer and Multilayer Graphene Electrodes. *J. Am. Chem. Soc.* **2012**, *134*, 7258–7261.
- (22) Kim, J.; Renault, C.; Nioradze, N.; Arroyo-Currás, N.; Leonard, K. C.; Bard, A. J. Electrocatalytic Activity of Individual Pt Nanoparticles Studied by Nanoscale Scanning Electrochemical Microscopy. *J. Am. Chem. Soc.* **2016**, *138*, 8560–8568.
- (23) Takahashi, Y.; Kumatani, A.; Shiku, H.; Matsue, T. Scanning Probe Microscopy for Nanoscale Electrochemical Imaging. *Anal. Chem.* **2017**, *89*, 342–357.
- (24) Kang, M.; Momotenko, D.; Page, A.; Perry, D.; Unwin, P. R. Frontiers in Nanoscale Electrochemical Imaging: Faster, Multifunctional, and Ultrasensitive. *Langmuir* **2016**, *32*, 7993–8008.
- (25) Bentley, C. L.; Kang, M.; Unwin, P. R. Nanoscale Surface Structure-Activity in Electrochemistry and Electrocatalysis. *J. Am. Chem. Soc.* **2019**, *141*, 2179–2193.
- (26) Bentley, C. L.; Edmondson, J.; Meloni, G. N.; Perry, D.; Shkirskiy, V.; Unwin, P. R. Nanoscale Electrochemical Mapping. *Anal. Chem.* **2019**, *91*, 84–108.
- (27) Güell, A. G.; Meadows, K. E.; Dudin, P. V.; Ebejer, N.; Macpherson, J. V.; Unwin, P. R. Mapping Nanoscale Electrochemistry

of Individual Single-Walled Carbon Nanotubes. *Nano Lett.* **2014**, *14*, 220–224.

(28) Kislenco, V. A.; Pavlov, S. V.; Kislenco, S. A. Influence of Defects in Graphene on Electron Transfer Kinetics: The Role of the Surface Electronic Structure. *Electrochim. Acta* **2020**, *341*, 136011–136021.

(29) Pavlov, S. V.; Nazmutdinov, R. R.; Fedorov, M. V.; Kislenco, S. A. Role of Graphene Edges in the Electron Transfer Kinetics: Insight from Theory and Molecular Modeling. *J. Phys. Chem. C* **2019**, *123*, 6627–6634.

(30) Ramos, P.; Mankarious, M.; Pavanello, M. A Critical Look at Methods for Calculating Charge Transfer Couplings Fast and Accurately. In *Practical Aspects of Computational Chemistry IV*; Springer US: Boston, MA, 2016; pp 103–134.

(31) Kubas, A.; Gajdos, F.; Heck, A.; Oberhofer, H.; Elstner, M.; Blumberger, J. Electronic Couplings for Molecular Charge Transfer: Benchmarking CDFT, FODFT and FODFTB against High-Level Ab Initio Calculations. II. *Phys. Chem. Chem. Phys.* **2015**, *17*, 14342–14354.

(32) Genova, A.; Ceresoli, D.; Pavanello, M. Periodic Subsystem Density-Functional Theory. *J. Chem. Phys.* **2014**, *141*, No. 174101.

(33) Behara, P. K.; Dupuis, M. Electron Transfer in Extended Systems: Characterization by Periodic Density Functional Theory Including the Electronic Coupling. *Phys. Chem. Chem. Phys.* **2020**, *22*, 10609–10623.

(34) Nikitina, V. A.; Kislenco, S. A.; Nazmutdinov, R. R.; Bronshtein, M. D.; Tsirlina, G. A. Ferrocene/Ferrocenium Redox Couple at Au(111)/Ionic Liquid and Au(111)/Acetonitrile Interfaces: A Molecular-Level View at the Elementary Act. *J. Phys. Chem. C* **2014**, *118*, 6151–6164.

(35) Heller, I.; Kong, J.; Williams, K. A.; Dekker, C.; Lemay, S. G. Electrochemistry at Single-Walled Carbon Nanotubes: The Role of Band Structure and Quantum Capacitance. *J. Am. Chem. Soc.* **2006**, *128*, 7353–7359.

(36) Kresse, G.; Furthmüller, J. Efficiency of Ab-Initio Total Energy Calculations for Metals and Semiconductors Using a Plane-Wave Basis Set. *Comput. Mater. Sci.* **1996**, *6*, 15–50.

(37) Kresse, G.; Furthmüller, J. Efficient Iterative Schemes for Ab Initio Total-Energy Calculations Using a Plane-Wave Basis Set. *Phys. Rev. B* **1996**, *54*, No. 11169.

(38) Electrochemistry. <https://github.com/vitalyanich/electrochemistry> (accessed February 26, 2020).

(39) Kuznetsov, A. M.; Nazmutdinov, R. R.; Schmickler, W. Monte Carlo Simulation of Electrochemical Electron Transfer Processes. *J. Electroanal. Chem.* **2002**, *532*, 171–180.

(40) Kuznetsov, A. M.; Ulstrup, J. *Electron Transfer in Chemistry and Biology: An Introduction to the Theory*; Wiley, 1999.

(41) Landau, L. D. On the Theory of Transfer of Energy at Collisions II. *Phys. Z. Sowjetunion* **1932**, *2*, 118.

(42) Zener, C. Non-Adiabatic Crossing of Energy Levels. *Proc. R. Soc. London, Ser. A* **1932**, *137*, 696–702.

(43) Gerischer, H. Charge Transfer Processes at Semiconductor-Electrolyte Interfaces in Connection with Problems of Catalysis. *Surf. Sci.* **1969**, *18*, 97–122.

(44) Trasatti, S. The Absolute Electrode Potential: An Explanatory Note. *Pure Appl. Chem.* **1986**, *58*, 955–966.

(45) Bard, A. J.; Faulkner, L. R. *Electrochemical Methods: Fundamentals and Applications*, 2nd ed.; John Wiley & Sons, 2001; pp 580–632.

(46) Legesse, M.; El Mellouhi, F.; Bentría, E. T.; Madjet, M. E.; Fisher, T. S.; Kais, S.; Alharbi, F. H. Reduced Work Function of Graphene by Metal Adatoms. *Appl. Surf. Sci.* **2017**, *394*, 98–107.

(47) Pavlov, S. V.; Kislenco, S. A. Graphene Electrochemistry: Edge vs. Basal Plane Sites. *J. Phys.: Conf. Ser.* **2018**, *1092*, No. 012112.

(48) Hoffmann, R. An Extended Hückel Theory. I. Hydrocarbons. *J. Chem. Phys.* **1963**, *39*, 1397–1412.

(49) Gajdos, F.; Valner, S.; Hoffmann, F.; Spencer, J.; Breuer, M.; Kubas, A.; Dupuis, M.; Blumberger, J. Ultrafast Estimation of

Electronic Couplings for Electron Transfer between  $\pi$ -Conjugated Organic Molecules. *J. Chem. Theory Comput.* **2014**, *10*, 4653–4660.

(50) Mándi, G.; Palotás, K. Chen's Derivative Rule Revisited: Role of Tip-Orbital Interference in STM. *Phys. Rev. B* **2015**, *91*, No. 165406.

(51) Tersoff, J.; Hamann, D. R. Theory of the Scanning Tunneling Microscope. *Phys. Rev. B* **1985**, *31*, No. 805.

(52) Chen, C. J. *Introduction to Scanning Tunneling Microscopy*, 2nd ed.; Oxford University Press: New York, 2007.

(53) Pavlov, S. V.; Kislenco, S. A. Effects of Carbon Surface Topography on the Electrode/Electrolyte Interface Structure and Relevance to Li-Air Batteries. *Phys. Chem. Chem. Phys.* **2016**, *18*, 30830–30836.

(54) Kislenco, S. A.; Amirov, R. H.; Samoylov, I. S. Effect of Cations on the TiO<sub>2</sub>/Acetonitrile Interface Structure: A Molecular Dynamics Study. *J. Phys. Chem. C* **2013**, *117*, 10589–10596.

(55) Pavlov, S. V.; Kislenco, S. A. Investigation of the Graphene-Electrolyte Interface in Li-Air Batteries: A Molecular Dynamics Study. *J. Phys.: Conf. Ser.* **2018**, *946*, No. 012028.

(56) Blöchl, P. E. Projector Augmented-Wave Method. *Phys. Rev. B* **1994**, *50*, No. 17953.

(57) Zhan, C.; Neal, J.; Wu, J.; Jiang, D. E. Quantum Effects on the Capacitance of Graphene-Based Electrodes. *J. Phys. Chem. C* **2015**, *119*, 22297–22303.

(58) Peover, M. E.; White, B. S. Electrolytic Reduction of Oxygen in Aprotic Solvents: The Superoxide Ion. *Electrochim. Acta* **1966**, *11*, 1061–1067.

(59) Belova, A. I.; Kwabi, D. G.; Yashina, L. V.; Shao-Horn, Y.; Itkis, D. M. Mechanism of Oxygen Reduction in Aprotic Li-Air Batteries: The Role of Carbon Electrode Surface Structure. *J. Phys. Chem. C* **2017**, *121*, 1569–1577.

(60) Laoire, C. O.; Mukerjee, S.; Abraham, K. M.; Plichta, E. J.; Hendrickson, M. A. Elucidating the Mechanism of Oxygen Reduction for Lithium-Air Battery Applications. *J. Phys. Chem. C* **2009**, *113*, 20127–20134.

(61) Lebedeva, M. V.; Pierron-Bohnes, V.; Goyhenex, C.; Papaefthimiou, V.; Zafeiratos, S.; Nazmutdinov, R. R.; Da Costa, V.; Acosta, M.; Zosiak, L.; Kozubski, R.; Mullere, D.; Savinova, E. R. Effect of the Chemical Order on the Electrocatalytic Activity of Model PtCo Electrodes in the Oxygen Reduction Reaction. *Electrochim. Acta* **2013**, *108*, 605–616.

(62) Lide, D. R. *CRC Handbook of Chemistry and Physics*; CRC Press, 2004.

(63) Smalley, J. F.; Finklea, H. O.; Chidsey, C. E. D.; Linford, M. R.; Creager, S. E.; Ferraris, J. P.; Chalfant, K.; Zawodzinski, T.; Feldberg, S. W.; Newton, M. D. Heterogeneous Electron-Transfer Kinetics for Ruthenium and Ferrocene Redox Moieties through Alkanethiol Monolayers on Gold. *J. Am. Chem. Soc.* **2003**, *125*, 2004–2013.

(64) Slowinski, K.; Slowinska, K. U.; Majda, M. Electron Tunneling Across Hexadecanethiolate Monolayers on Mercury Electrodes: Reorganization Energy, Structure, and Permeability of the Alkane/Water Interface. *J. Phys. Chem. B* **1999**, *103*, 8544–8551.

(65) Ma, J.; Alfè, D.; Michaelides, A.; Wang, E. Stone-Wales Defects in Graphene and Other Planar Sp<sup>2</sup>-Bonded Materials. *Phys. Rev. B* **2009**, *80*, No. 033407.

(66) Openov, L. A.; Podlivaev, A. I. Real-Time Evolution of the Buckled Stone-Wales Defect in Graphene. *Physica E* **2015**, *70*, 165–169.

(67) Vanević, M.; Stojanović, V. M.; Kindermann, M. Character of Electronic States in Graphene Antidot Lattices: Flat Bands and Spatial Localization. *Phys. Rev. B* **2009**, *80*, No. 045410.

(68) Wang, S.; Talirz, L.; Pignedoli, C. A.; Feng, X.; Müllen, K.; Fasel, R.; Ruffieux, P. Giant Edge State Splitting at Atomically Precise Graphene Zigzag Edges. *Nat. Commun.* **2016**, *7*, No. 11507.

(69) Ugeda, M. M.; Brihuega, I.; Guinea, F.; Gómez-Rodríguez, J. M. Missing Atom as a Source of Carbon Magnetism. *Phys. Rev. Lett.* **2010**, *104*, No. 096804.

(70) Newns, D. M. Self-Consistent Model of Hydrogen Chemisorption. *Phys. Rev.* **1969**, *178*, No. 1123.

(71) Zacharov, I.; Arslanov, R.; Gunin, M.; Stefonishin, D.; Bykov, A.; Pavlov, S.; Panarin, O.; Maliutin, A.; Rykovanov, S.; Fedorov, M. “Zhores”—Petaflops Supercomputer for Data-Driven Modeling, Machine Learning and Artificial Intelligence Installed in Skolkovo Institute of Science and Technology. *Open Eng.* **2019**, *9*, 512–520.